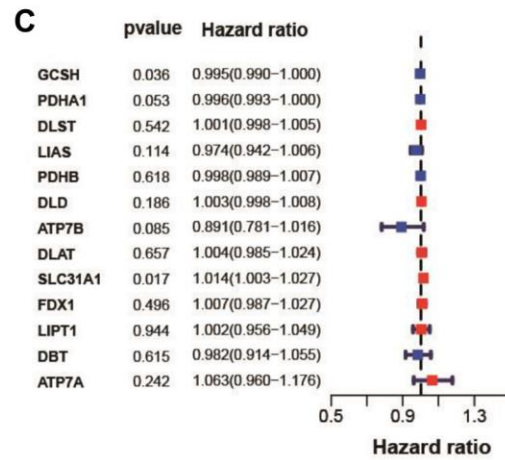
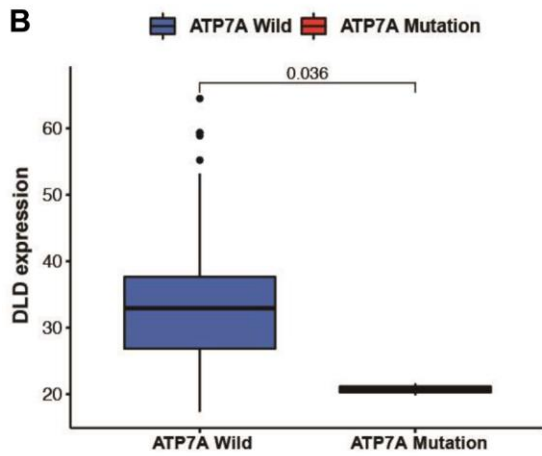
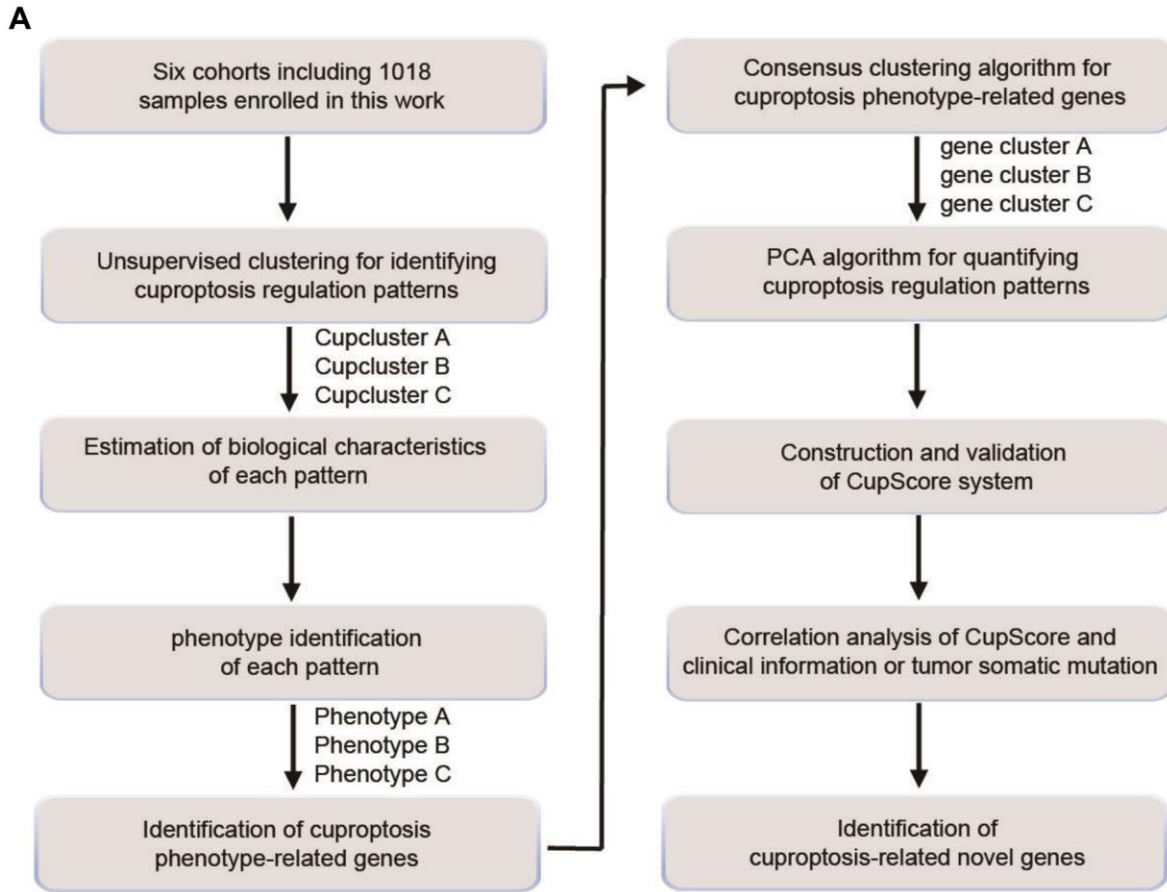
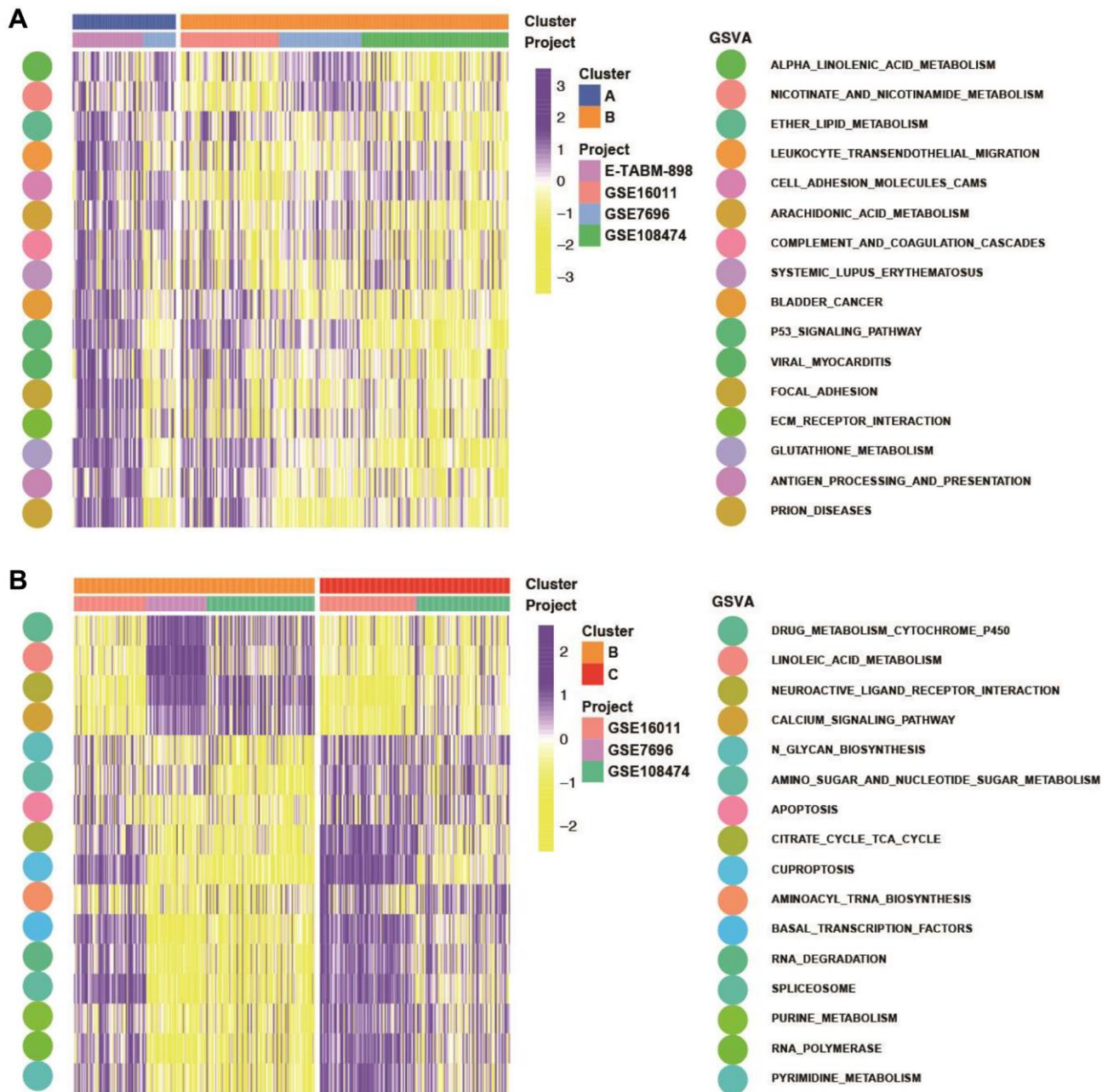


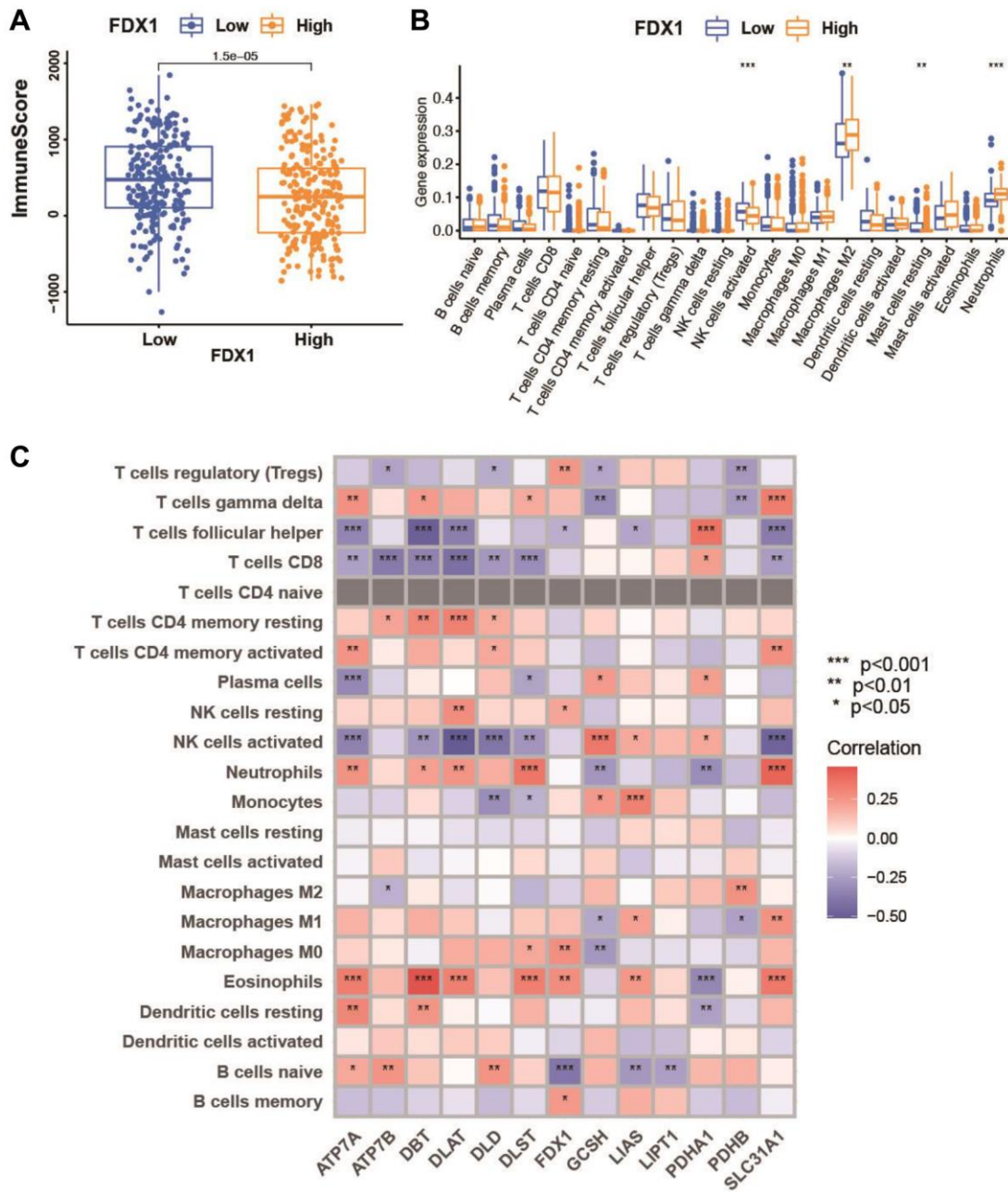
SUPPLEMENTARY FIGURES



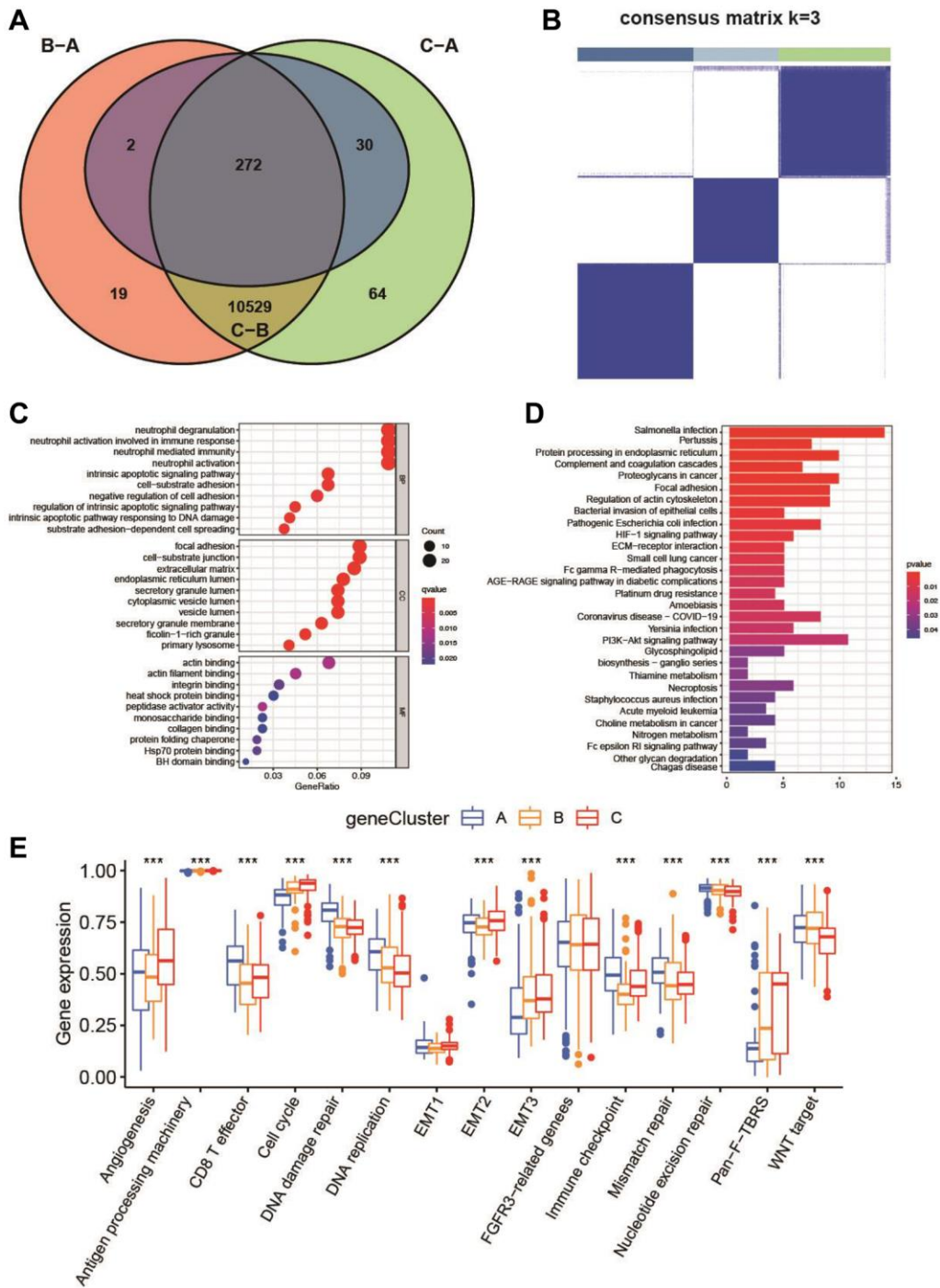
Supplementary Figure 1. Overview of study design and prognostic analysis of 13 cuproptosis regulators. (A) Overview of this work. (B) Expression differences of DLD between ATP7A wild and ATP7A mutation in TCGA and CGGA cohorts. (C) The prognostic analyses for 13 cuproptosis regulators in TCGA and CGGA cohorts using a univariate Cox regression model.



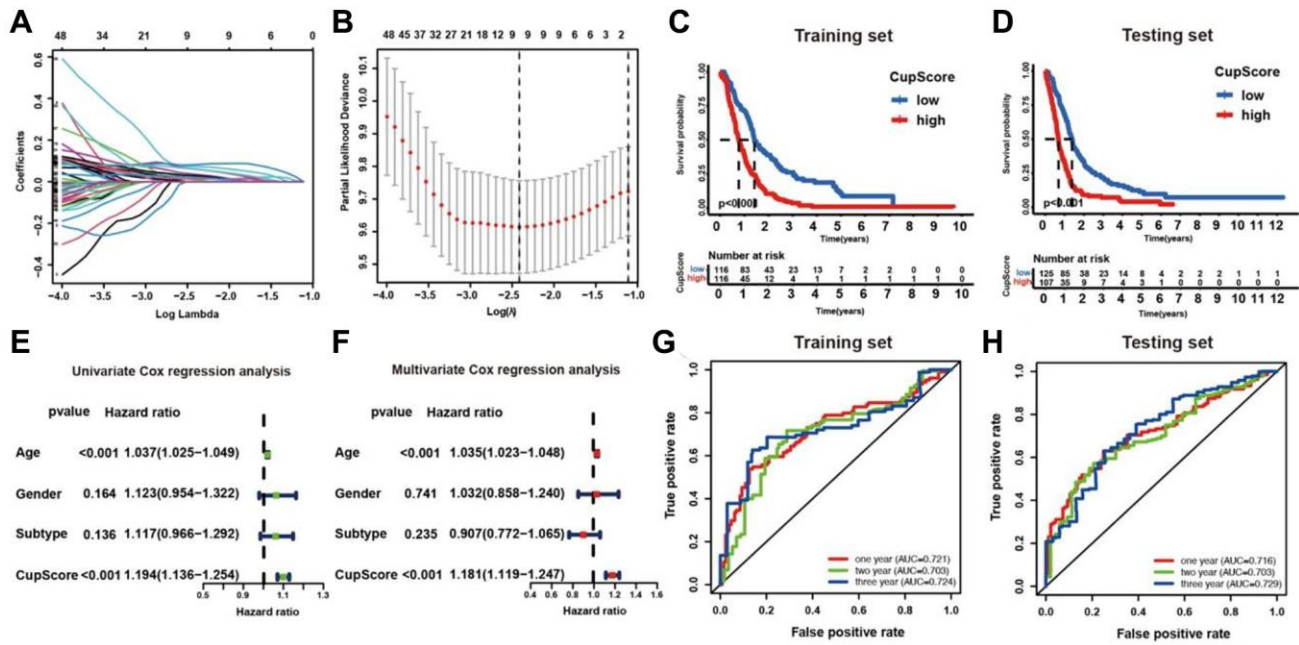
Supplementary Figure 2. Biological characteristics of cuproptosis regulation pattern. (A) GSEA enrichment analysis showing the activation biological pathways between cuproptosis regulation patterns A and B. Purple: activated pathways; yellow: inhibited pathways. The GBM cohorts were used as sample annotations (GSE7696, GSE16011, GSE108474, ArrayExpress-E-TABM-898). (B) GSEA enrichment analysis showing the activation biological pathways between cuproptosis regulation patterns B and C. Purple: activated pathways; yellow: inhibited pathways. The GBM cohorts were used as sample annotations (GSE7696, GSE16011, GSE108474, ArrayExpress-E-TABM-898).



Supplementary Figure 3. Correlation analysis between TME infiltrating cells and cuproptosis regulators. (A) Expression differences of ImmuneScore in high- and low-FDX1 expression and mutation in four GBM cohorts. (B) Difference in the abundance of each TME infiltrating cell between FDX1 high expression and low expression groups. (C) The correlation between each cuproptosis regulator and each TME infiltration cell type. Red: positive correlation; Purple: negative correlation.



Supplementary Figure 4. Identification and functional annotation of cuproptosis pattern related DEGs. (A) Venn diagram indicating cuproptosis-related genes identified in three patterns. (B) Unsupervised clustering of 205 cuproptosis regulation pattern related DEGs and consensus matrices for $k = 3$, which was the optimal cluster number in four GBM cohorts. (C, D) Functional annotation for cuproptosis-related genes using GO and KEGG enrichment analysis. The color depth of the barplots represented the number of genes enriched. (E) Difference in the expression of known signatures including stromal-activation related signatures among three gene clusters. significant results are indicated as $*p < 0.05$, $**p < 0.01$, and $***p < 0.001$.



Supplementary Figure 5. Construction and validation of cuproptosis gene signature. (A) LASSO coefficient profiles of the cuproptosis regulation pattern related DEGs in the training set. (B) A coefficient profile plot was generated against the log (lambda) sequence. Selection of the optimal parameter (lambda) in the LASSO model. (C) Survival analyses for low (116 cases) and high (116 cases) CupScore patient groups in training cohort using Kaplan-Meier curves. (D) Survival analyses for low (125 cases) and high (107 cases) CupScore patient groups in testing cohort using Kaplan-Meier curves. (E, F) Forest plot showing univariate and multivariate Cox regression analyses of CupScore associated with age, gender, subtype and CupScore of two cohorts. (G, H) The predictive value of the quantification of cuproptosis gene signatures in training cohort (AUC, 0.721) and testing cohort (AUC, 0.716).